Tapered Optical Fiber Sensor for Discrimination of Strain and Temperature

Mustafa BILSEL, Isa NAVRUZ

Department of Electrical and Electronics Engineering, Faculty of Engineering, Ankara University, Golbasi 50, Yil Yerleskesi, 06830 Golbasi/Ankara, Turkey

mbilsel@ankara.edu.tr, inavruz@ankara.edu.tr

Abstract. *A simple Mach-Zehnder Interferometer (MZI) based on a standard single-mode fiber for simultaneous strain and temperature sensing was proposed and demonstrated experimentally. The interferometer was fabricated by electrical arc discharge method in which a part of the standard single-mode fiber was heated and stretched. Any special type of fiber or a particular splicer was not required to form the MZI and it indicated high resolution. To find the modes that contributed to the interference spectrum, Fourier analysis was done and the spatial frequency versus normalized intensity plot showed that LP02 was the excited dominant higher order cladding mode. Coefficient matrix was realized for simultaneous measurement of strain and temperature ability of such an MZI. For discrete measurements, a resolution of 0.79 °C and 1.18 microstrain can be achieved for 10 pm wavelength resolution. This extremely simple, low-cost sensor easily fabricated with good repeatability is a good candidate in diverse sensing applications.*

Keywords

Fourier analysis, strain sensing, tapered fiber, temperature sensing.

1. Introduction

Tapered fiber sensors have some superior features compared to electrical sensors such as small size, immunity to electromagnetic interference, remote sensing, simple fabrication, low cost, ability to operate in harsh environments and simultaneous measurement of more than one parameter. Refractive Index (RI) [1] and [2], pressure [3] and [4], temperature [5] and [6], stress [7] and [8] and chemical and biological sensing [9], [10], [11] and [12] are the most commonly studied parameters in the literature to characterize the sensor's response. Recently, Lu et al. [5] proposed a tapered MZI for simultaneous measurement of RI and temperature. A commercial splicer was used to fabricate the sensor, which had a waist diameter of 65 μm and a length of 525 μm. They achieved temperature and RI sensitivities of 0.077 nm·°C^{-1} and -26.087 nm·RIU^{-1}, respectively. Tian et al. [13] proposed an MZI with two abrupt single-mode fiber tapers for strain measurements. They fabricated the sensor by a commercial fusion splicer with the following parameters: waist diameter and length were 40 μm and 707 μm, respectively. Strain sensitivity of 2 pm·με^{-1} was obtained; it is low because of the limitations of the splicer both in waist diameter and length. In another study by Andre et al. [14], a coreless multimode fiber was spliced between single-mode fibers and tapered. The sensors with different waist diameters of 15 μm, 25 μm, 55 μm, 74 μm and 87 μm were analyzed in terms of their strain and temperature response. The highest strain sensitivity of -23.7 pm·με^{-1} was obtained for the thinnest waist diameter. Temperature sensitivities of 16.56 pm·°C^{-1} and 13.95 pm·°C^{-1} were obtained for 87 μm and 25 μm tapers, respectively. Kieu et al. [15] fabricated a biconical fiber taper from a standard telecom single-mode fiber with diameter of about 10 μm to sense displacement, temperature and RI. The sensor was thin enough to sense displacement and RI. They obtained resolutions of 0.1 μm, 1 °C and $1.42 \cdot 10^{-5}$ RI unit for displacement, temperature and RI, respectively.

In this study, an MZI based on a standard telecom single-mode fiber is investigated for simultaneous measurement of strain and temperature. The interferometer was fabricated by arc discharge method in which a section of fiber was heated and pulled by a completely computer-controlled setup. Excited higher-order modes and fundamental mode contribute to in-

terference spectrum. For discrete measurements, resolutions of 0.79 °C and 1.18 με were determined for strain and temperature, respectively.

2. Sensing Principle

Schematic illustration and microscopic image of the tapered fiber were shown in Fig. 1(a) and Fig. 1(b), respectively. When light propagating in untapered fiber meets up the first transition region, a part of its energy will split into two parts; one as a cladding mode, second as a core mode. Waist region behaves as an interaction region in which light interacts with surrounding medium. The second transition region acts as an optical coupler whose role is to modulate interference pattern between core and cladding modes. Due to the optical path difference between core and one of the cladding modes, a phase difference occurs [16]:

$$\varphi = \frac{2\pi\Delta n_{eff}L}{\lambda},\qquad(1)$$

where $\Delta n_{eff} = n_{eff}^{co} - n_{eff}^{cl}$ is the effective RI difference between core and the cladding mode, L is the waist length, λ is the wavelength. When phase difference becomes equal to $(2m+1)\lambda$, destructive interference occurs so expression for resultant corresponding dip wavelength follows as [17]:

$$\lambda_{dip} = \frac{2\pi\Delta n_{eff}L}{2m+1}.\qquad(2)$$

Different types of modes supported by the taper will be excited because of change in the environmental conditions of the surrounding medium so either blue-shift or red-shift will be observed depending on the surrounding parameter.
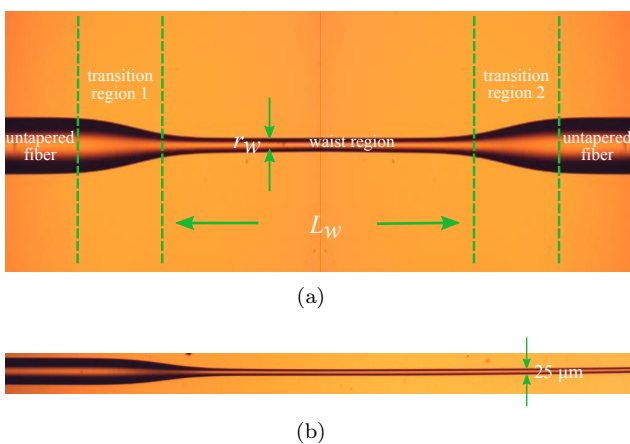

Fig. 1: Schematic illustration (a) and microscopic image (b) of the tapered fiber.

3. Results

In this experiment, tapered fiber was fabricated by using arc discharge method which is mainly based on stretching a portion of fiber while heating it to its softening temperature. Experimental setup used to fabricate a tapered fiber is shown in Fig. 2. After stripping the primary coating of the fiber, one end of the fiber was fixed by a fiber holder. The other end of the fiber is mounted on a moving stage which is responsible for stretching the fiber when it is heated. The moving stage is controlled by a stepper which generates axial motion resolution of 1.25 μm at each step. Electrodes are placed on another moving stage whose motion is controlled by another identical stepper. To reach the softening point of the fiber, a series of arc pulses are applied for a short time via electrodes. Meanwhile, steppers start to move in opposite direction; one stretching the fiber at a higher speed and the other moving the electrodes at a lower speed. Computer software controls acceleration and speed of moving stages, pulse duration and instantaneous arc power so that a sensor with desired waist diameter and length can be fabricated. When compared against fabrication via commercial splicer, there is no restriction on length of the sensor but steppers in fusion splicers are capable of moving about 1 mm.
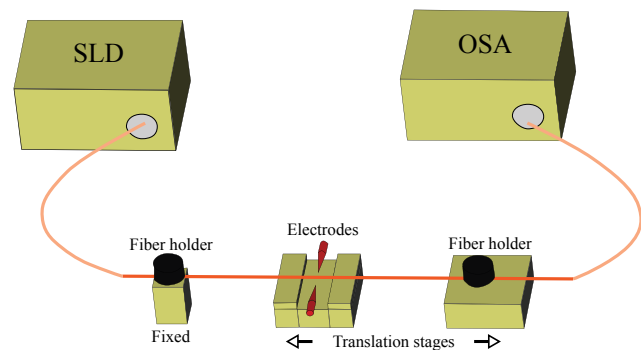

Fig. 2: Experimental setup for sensor fabrication.

Referring to Fig. 1, the sensor head had the following parameters; waist diameter (r_w) and length (L_w) were 25 μm and 29 mm, respectively. The reason for the choice of that waist length is to decrease fringe spacing so that more than two dips will be formed to measure the resolution of sensor in strain and temperature measurements. In the case of waist diameter, setup in Fig. 2 can achieve uniform waist diameter down to 6 μm. Further decrease in chosen waist diameter, 25 μm, becomes core region substantially lost and repeated experiments have shown that sensor's response to temperature has been adversely affected. In the setup, the desired waist length is well controlled by the micrometer steps of the motor on the right stage. The uniform waist diameter simultaneously requires not only to set the speed of the motors with

appropriate values, but also to ensure the stability of the arc power. The waist diameter is an important parameter to form wavelength spectrum so it directly affects the sensitivity. To evaluate the reproducibility, 10 samples were fabricated with waist diameter of 25 μm and relative standard deviation was calculated as 2.2 %. It should be noted that reproducibility is strongly affected by the precise measurement of waist diameter from microscopic image. To characterize the MZI, light from a Super Luminescent Diode (SLD) source with a range of 1450–1650 nm was injected to the sensor and the interference spectrum was recorded by an optical spectrum analyzer. At room temperature, typical transmission spectrum in the air was shown in Fig. 3. Spectrum shows sinusoidal oscillations due to strong interference between cladding mode and the fundamental mode. For strain and temperature measurements, three peaks called dipA, dipB and dipC located at 1555.8, 1580.9 and 1607.6 nm were followed.
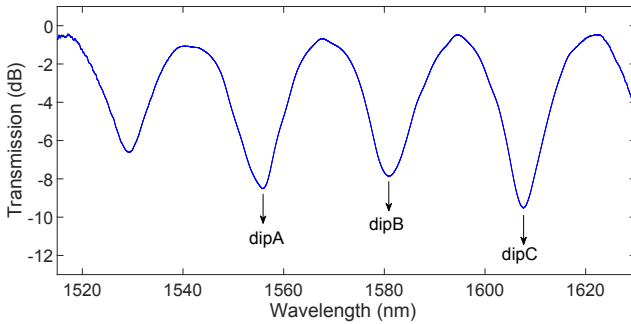

Fig. 3: Typical transmission spectrum of the sensor in the air.

Fast Fourier transform of the transmission spectrum given in Fig. 3 was taken to determine the dominant cladding mode that contributed to interference. The spatial frequency spectrum of the interference pattern was shown in Fig. 4. Line with peak amplitude of 1 corresponds to the fundamental mode and the following peak indicates the existence of a dominant cladding mode. To decide on the type of the excited cladding mode, effective RI difference between cladding and fundamental mode can be compared analytically and experimentally. To do this, Beam Propagation Method (BPM) simulations were carried out and compared with experimental results. Taylor expansion of Eq. (1) at the center wavelength of λ_c, wavelength spacing between two adjacent dips, can be expressed as [18]:

$$\Lambda = \frac{\lambda_c^2}{\Delta n_{eff} L}. \tag{3}$$

By taking $L = 29$ mm, $\lambda_c = 1568$ nm and the average spacing $\Lambda = 25.6$ nm, experimental effective RI difference was calculated as $3.32 \cdot 10^{-3}$. On the other hand, BPM analysis showed that effective RI difference between the fundamental mode and LP02 mode

was equal to $3.39 \cdot 10^{-3}$. Therefore, it is verified that LP_{02} mode is the dominant mode that interferes with the fundamental mode.
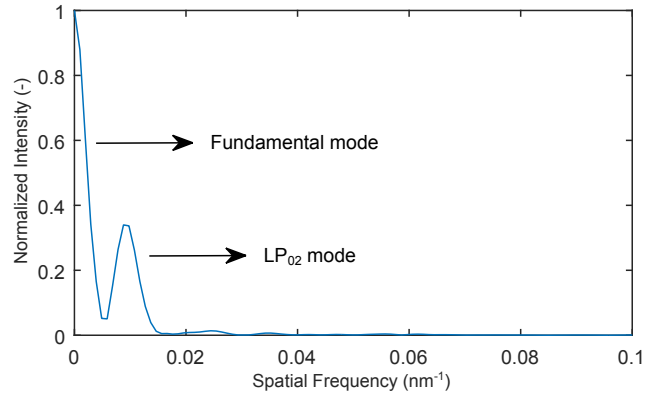

Fig. 4: Fast Fourier transform of transmission spectrum in the air.

For strain measurements, the temperature of the surrounding medium was kept constant. One end of the sensor was fixed and the other end was attached to a stepper motor. In order to apply stress on the sensor by micro-step distances, sensor end connected to the stepper motor was moved and a strain of 124 με was created at each time. As strain was increased, the spectrum exhibited blue-shifts as shown in Fig. 5(a). Enlarged views of wavelength shifts in dipA, dipB and dipC were shown in Fig. 6. Corresponding total spectral shifts of dipA, dipB and dipC were 9.1, 9.2 and 9.3 nm, respectively, when strain in the range 0–1116 με was applied. Sensitivities of 8.4665 pm·με^{-1}, 8.1892 pm·με^{-1}, 8.4604 pm·με^{-1} were obtained for dipA, dipB and dipC, respectively (Fig. 5(b)).

Since the sensor was too sensitive to strain, during temperature measurement experiments, the sensor was laid freely on a flat surface not to change the strain because of thermal expansion. In this way, strain effect was eliminated during temperature measurements. Temperature response of the sensor was examined by inserting the sensor in an oven which was capable of controlling temperature in the range between room temperature and 150 °C with a resolution of 0.1 °C. Figure 7(a) shows the sensor's response to temperature. It is clearly seen that all spectrum dips experience red-shift linearly with increasing temperature. Enlarged views of sensor dips were plotted in Fig. 8 where all the dips showed similar behaviour. Temperature sensitivities were obtained by linear fitting to measured data points and sensitivities of 12.496 pm·°C^{-1}, 12.623 pm·°C^{-1} and 11.028 pm·°C^{-1} were obtained for dipA, dipB and dipC, respectively (Fig. 7(b)).

To examine the effect of applying the strain and temperature simultaneously, it is necessary to monitor the wavelength shift of two dips. Since each dip has a dif-
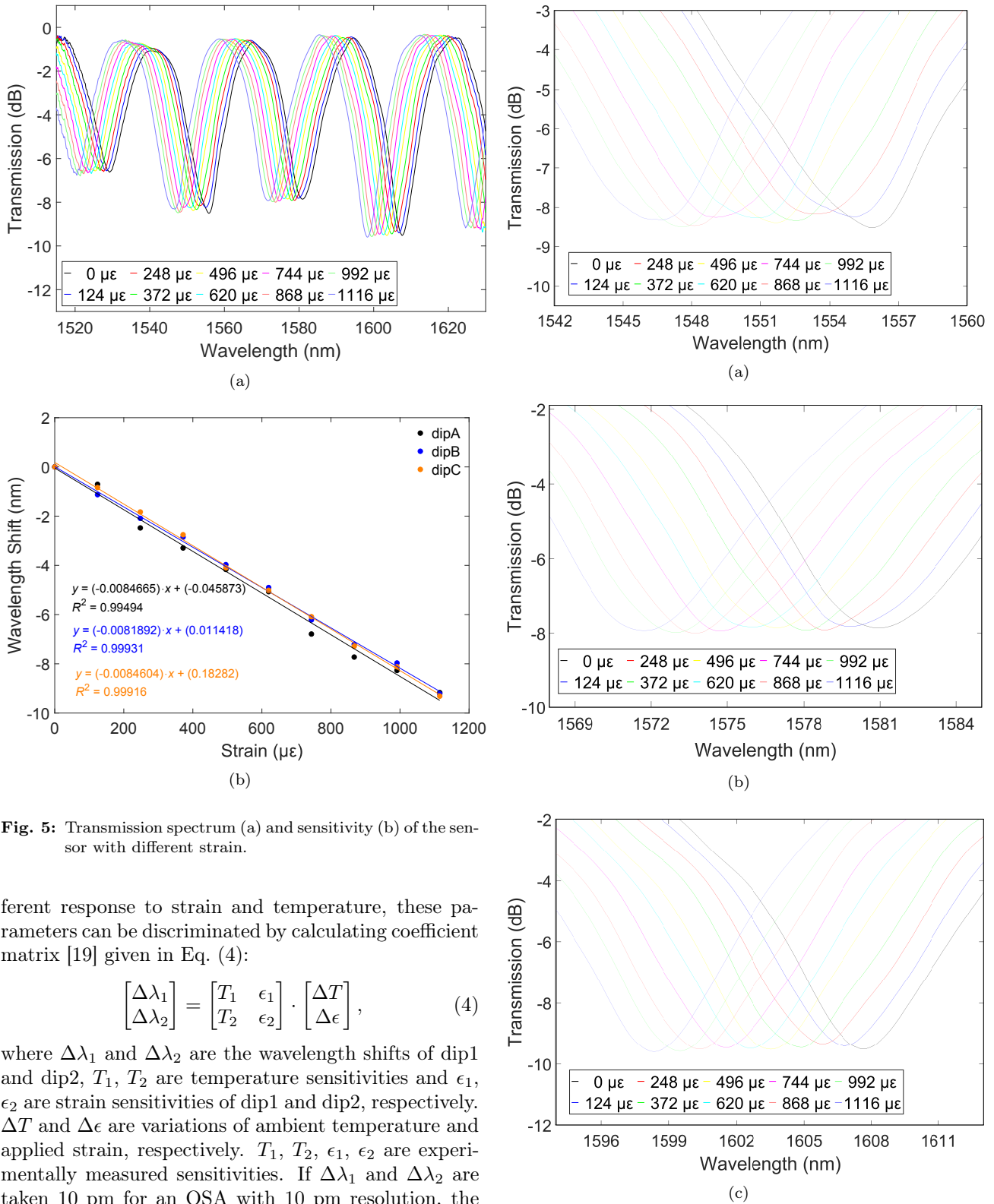
(a)

(b)

Fig. 5: Transmission spectrum (a) and sensitivity (b) of the sensor with different strain.

(a)

(b)

(c)

Fig. 6: Enlarged views of wavelength shifts for (a) dipA, (b) dipB and (c) dipC due to strain.

ferent response to strain and temperature, these parameters can be discriminated by calculating coefficient matrix [19] given in Eq. (4):

$$\begin{bmatrix} \Delta \lambda_1 \\ \Delta \lambda_2 \end{bmatrix} = \begin{bmatrix} T_1 & \epsilon_1 \\ T_2 & \epsilon_2 \end{bmatrix} \cdot \begin{bmatrix} \Delta T \\ \Delta \epsilon \end{bmatrix}, \qquad (4)$$

where $\Delta \lambda_1$ and $\Delta \lambda_2$ are the wavelength shifts of dip1 and dip2, T_1, T_2 are temperature sensitivities and ϵ_1, ϵ_2 are strain sensitivities of dip1 and dip2, respectively. ΔT and $\Delta \epsilon$ are variations of ambient temperature and applied strain, respectively. T_1, T_2, ϵ_1, ϵ_2 are experimentally measured sensitivities. If $\Delta \lambda_1$ and $\Delta \lambda_2$ are taken 10 pm for an OSA with 10 pm resolution, the spectral resolution of the sensor can be calculated by the inverse matrix method. For dipB and dipC, the coefficient matrix can be written as:

$$\begin{bmatrix} \Delta \lambda_B \\ \Delta \lambda_C \end{bmatrix} = \begin{bmatrix} 12.623 & -8.1892 \\ 11.028 & -8.4604 \end{bmatrix} \cdot \begin{bmatrix} \Delta T \\ \Delta \epsilon \end{bmatrix}, \qquad (5)$$

where $\Delta \lambda_B$ and $\Delta \lambda_C$ represent wavelength shifts of dipB and dipC, respectively. For an OSA with reso-

lution of 10 pm, the resolution of the sensor was calculated as 10.09 °C and 14.34 με for temperature and strain, respectively. It is likely that high-temperature
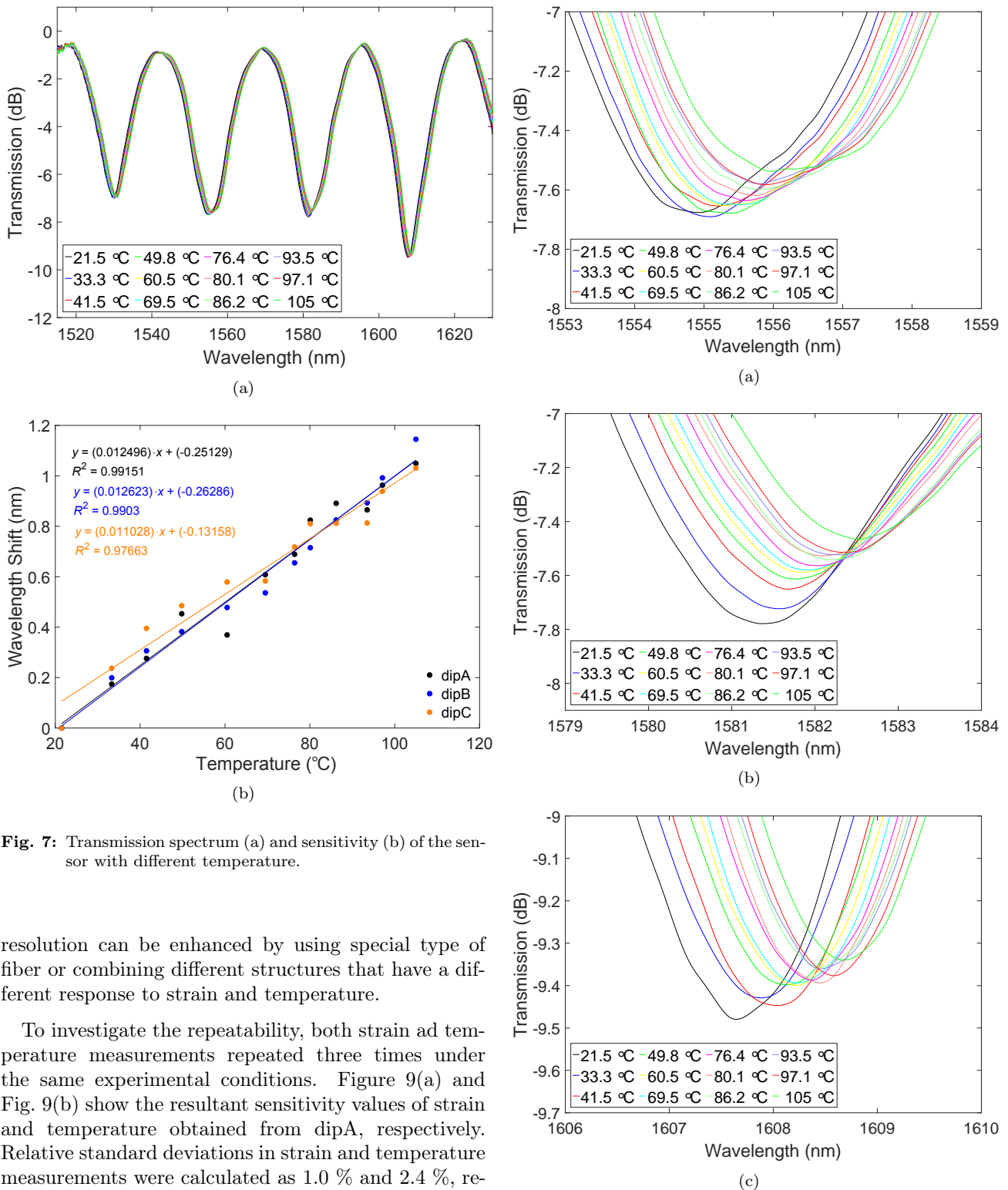
(a)

(b)

Fig. 7: Transmission spectrum (a) and sensitivity (b) of the sensor with different temperature.

resolution can be enhanced by using special type of fiber or combining different structures that have a different response to strain and temperature.

To investigate the repeatability, both strain ad temperature measurements repeated three times under the same experimental conditions. Figure 9(a) and Fig. 9(b) show the resultant sensitivity values of strain and temperature obtained from dipA, respectively. Relative standard deviations in strain and temperature measurements were calculated as 1.0 % and 2.4 %, respectively. Similar results were obtained for dipB and dipC. The results indicate that the proposed sensor has good repeatability.

A comparison is carried out between the proposed sensor and the sensors in references which measure either strain or temperature. Unlike the sensors in [5], [8] and [13], waist diameter of the proposed sensor is thinner, which makes it more sensitive to strain because strain depends on cross-sectional area of waist re-

(a)

(b)

(c)

Fig. 8: Enlarged views of wavelength shifts for (a) dipA, (b) dipB and (c) dipC due to temperature.

gion. Those sensors were fabricated by a fusion splicer whose stepper has restricted to move 1 mm and electrodes were stationary. On the other hand, unlike the fusion splicer, electrodes are movable with appropriate
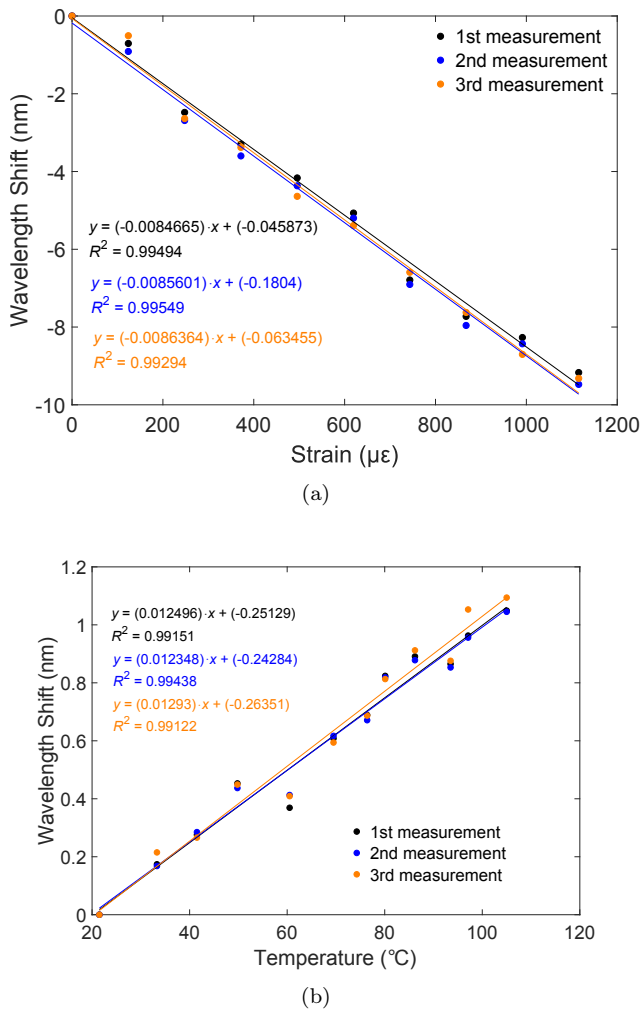
$y = (-0.0084665) \cdot x + (-0.045873)$
$R^2 = 0.99494$

$y = (-0.0085601) \cdot x + (-0.1804)$
$R^2 = 0.99549$

$y = (-0.0086364) \cdot x + (-0.063455)$
$R^2 = 0.99294$

(a)

$y = (0.012496) \cdot x + (-0.25129)$
$R^2 = 0.99151$

$y = (0.012348) \cdot x + (-0.24284)$
$R^2 = 0.99438$

$y = (0.01293) \cdot x + (-0.26351)$
$R^2 = 0.99122$

(b)

Fig. 9: Results of repeated (a) strain and (b) temperature experiments.

speed and acceleration, which allows fabricating a sensor with uniform and longer waist. Reference [6] employs a commercial tapering machine which increases cost. Besides, relevant sensors mentioned above can measure either strain or temperature. Although the sensor in [15] can measure both strain and temperature, the proposed sensor has better resolution. Therefore, superiority of fabrication details mentioned above and enhanced resolution in strain and temperature improves performance, especially in terms of strain.

4. Conclusion

A simple MZI based on a standard telecom single-mode fiber for simultaneous measurement of strain and temperature was investigated and demonstrated experimentally. Experimental results indicated that temperature resolution of 0.79 °C and strain resolution of 1.18 µε were achieved for discrete measurements. For simultaneous measurements, resolutions of

10.09 °C and 14.34 µε were calculated by using the matrix method for temperature and strain, respectively. The interferometer does not require any special type of fiber and particular splicer for fabrication so it is cost-effective and simple to fabricate. In that respect, it can be a good choice both in discrete and simultaneous measurements of strain and temperature in various fields of related applications.

References

[1] JI, W. B., H. H. LIU, S. C. TJIN, K. K. CHOW and A. LIM. Ultrahigh Sensitivity Refractive Index Sensor Based on Optical Microfiber. *IEEE Photonics Technology Letters*. 2012, vol. 24, iss. 20, pp. 1872–1874. ISSN 1941-0174. DOI: 10.1109/LPT.2012.2217738.

[2] LACROIX, S., F. GONTHIER, R. J. BLACK and J. BURES. Tapered-fiber interferometric wavelength response: the achromatic fringe. *Optics Letters*. 1988, vol. 13, iss. 5, pp. 395–397. ISSN 1539-4794. DOI: 10.1364/OL.13.000395.

[3] BARIAIN, C., I. R. MATIAS, F. J. ARREGUI and M. LOPEZ-AMO. Tapered optical-fiber-based pressure sensor. *Optical Engineering*. 2000, vol. 39, iss. 8, pp. 2241–2247. ISSN 1560-2303. DOI: 10.1117/1.1304926.

[4] MASSARO, A., F. SPANO, M. MISSORI, M. A. MALVINDI, P. CAZZATO, R. CINGOLANI and A. ATHANASSIOU. Flexible nanocomposites with all-optical tactile sensing capability. *RCS Advances*. 2014, vol. 4, iss. 6, pp. 2820–2825. ISSN 2046-2069. DOI: 10.1039/C3RA45678A.

[5] LU, P., L. MEN, K. SOOLEY and Q. CHEN. Tapered fiber Mach–Zehnder interferometer for simultaneous measurement of refractive index and temperature. *Applied Physics Letters*. 2009, vol. 94, iss. 13, pp. 1–3. ISSN 1077-3118. DOI: 10.1063/1.3115029.

[6] HERNANDEZ-ROMANO, I., D. MONZON-HERNANDEZ, C. MORENO-HERNANDEZ, D. MORENO-HERNANDEZ and J. VILLA-TORO. Highly Sensitive Temperature Sensor Based on a Polymer-Coated Microfiber Interferometer. *IEEE Photonics Technology Letters*. 2015, vol. 27, iss. 24, pp. 2591–2594. ISSN 1941-0174. DOI: 10.1109/LPT.2015.2478790.

[7] SHAO, L.-Y., J. ZHAO, X. DONG, H. Y. TAM, C. LU and S. HE. Long-period grating fabricated by periodically tapering standard single-mode fiber. *Applied Optics*. 2007, vol. 47,

iss. 10, pp. 1549–1552. ISSN 2155-3165. DOI: 10.1364/AO.47.001549.

[8] YANG, R., Y.-S. YU, Y. XUE, C. CHEN, Q.-D. CHEN and H.-B. SUN. Single S-tapered fiber Mach–Zehnder interferometers. *Optics Letters.* 2011, vol. 36, iss. 23, pp. 4482–4484. ISSN 1539-4794. DOI: 10.1364/OL.36.004482.

[9] BARIAIN, C., I. R. MATIAS, C. FERNANDEZ-VALDIVIELSO, F. J. ARREGUI, M. L. RODRIGUEZ-MENDEZ and J. A. DE SAJA. Optical fiber sensor based on lutetium bisphthalocyanine for the detection of gases using standard telecommunication wavelengths. *Sensors and Actuators B: Chemical.* 2003, vol. 93, iss. 1–3, pp. 153–158. ISSN 0925-4005. DOI: 10.1016/S0925-4005(03)00204-1.

[10] CORRES, J. M., I. R. MATIAS, J. BRAVO and F. J. ARREGUI. Tapered optical fiber biosensor for the detection of anti-gliadin antibodies. *Sensors and Actuators B: Chemical.* 2008, vol. 135, iss. 1, pp. 166–171. ISSN 0925-4005. DOI: 10.1016/j.snb.2008.08.008.

[11] IRIGOYEN, M., J. A. SANCHEZ-MARTIN, E. BERNABEU and A. ZAMORA. Tapered optical fiber sensor for chemical pollutants detection in sea water. *Measurement Science and Technology.* 2017, vol. 28, no. 4, pp. 1-9. ISSN 1361-6501. DOI: 10.1088/1361-6501/aa5dc5.

[12] POSPISILOVA, M., G. KUNCOVA and J. TROGL. Fiber-Optic Chemical Sensors and Fiber-Optic Bio-Sensors. *Sensors.* 2015, vol. 15, iss. 10, pp. 25208–25259. ISSN 1424-8220. DOI: 10.3390/s151025208.

[13] TIAN, Z. and S. S.-H. YAM. In-Line Abrupt Taper Optical Fiber Mach–Zehnder Interferometric Strain Sensor. *IEEE Photonics Technology Letters.* 2009, vol. 21, iss. 3, pp. 161–163. ISSN 1941-0174. DOI: 10.1109/LPT.2008.2009360.

[14] ANDRE, R. M., C. R. BIAZOLI, S. O. SILVA, M. B. MARQUES, C. M. B. CORDEIRO and O. FRAZAO. Strain-Temperature Discrimination Using Multimode Interference in Tapered Fiber. *IEEE Photonics Technology Letters.* 2013, vol. 25, iss. 2, pp. 155–158. ISSN 1941-0174. DOI: 10.1109/LPT.2012.2230617.

[15] KIEU, K. Q. and M. MANSURIPUR. Biconical Fiber Taper Sensors. *IEEE Photonics Technology Letters.* 2006, vol. 18, iss. 21, pp. 2239–2241.

ISSN 1941-0174. DOI: 10.1109/LPT.2006.884742.

[16] TIAN, Z., S. S.-H. YAM and H.-P. LOOCK. Refractive index sensor based on an abrupt taper Michelson interferometer in a single-mode fiber. *Optics Letters.* 2008, vol. 33, iss. 10, pp. 1105–1107. ISSN 1539-4794. DOI: 10.1364/OL.33.001105.

[17] XIA, T.-H., A. P. ZHANG, B. GU and J.-J. ZHU. Fiber-optic refractive-index sensors based on transmissive and reflective thin-core fiber modal interferometers. *Optics Communications.* 2010, vol. 283, iss. 10, pp. 2136–2139. ISSN 0030-4018. DOI: 10.1016/j.optcom.2010.01.031.

[18] GENG, Y., X. LI, X. TAN, Y. DENG and Y. YU. High-Sensitivity Mach–Zehnder Interferometric Temperature Fiber Sensor Based on a Waist-Enlarged Fusion Bitaper. *IEEE Sensors Journal.* 2011, vol. 11, iss. 11, pp. 2891–2894. ISSN 1558-1748. DOI: 10.1109/JSEN.2011.2146769.

[19] ZHOU, D.-P., L. WEI, W.-K. LIU, Y. LIU and J. W. Y. LIT. Simultaneous measurement for strain and temperature using fiber Bragg gratings and multimode fibers. *Applied Optics.* 2008, vol. 47, iss. 10, pp. 1668–1672. ISSN 2155-3165. DOI: 10.1364/AO.47.001668.

About Authors

Mustafa BILSEL received his B.Sc. and M.Sc. degrees in Physics Engineering from Middle East Technical University and Ankara University in 1997 and 2007, respectively. He is currently a Ph.D. student in the Department of Electrical and Electronics Engineering in Ankara University. His current research interest is focused on tapered optical fiber sensors and fiber grating sensors.

Isa NAVRUZ was born in Turkey, in 1974. He received the B.Sc. degree in electrical and Electronics Engineering from Dokuz Eylul University, Izmir, in 1995 and the M.Sc. and Ph.D. degrees from Gazi University, Ankara, Turkey, in 2000 and 2006, respectively. He is currently an Associate Professor and the head of Optoelectronics and Photonics Research Group in Ankara University, Ankara, Turkey. His research interests include the design and characterization of optical fiber gratings, simulation of linear and nonlinear pulse propagation in optical fiber and design and application of optical fiber sensors.